Flexible High Efficiency Battery-Ready PV Inverter for Rooftop Systems

Namwon Kim, Mehrdad Biglarbegian, Babak Parkhideh
Electrical and Computer Engineering Department
Energy Production & Infrastructure Center (EPIC)
University of North Carolina at Charlotte
Charlotte, North Carolina, USA
Email: {nkim22, mbiglarb, bparkhideh}@uncc.edu

***Abstract*—Integration of energy storage with a grid-tied photovoltaic (PV) generation system in conventional residential and commercial applications uses legacy PV power electronics topologies. This paper presents a novel solar PV power electronics system which allows a seamless integration of energy storage with partial power processing technique. In the proposed topology, a dual active bridge DC-DC converter is applied to configure partially-rated power electronics system with bi-directional power flow, galvanic isolation, a high voltage boosting gain, and results in high conversion efficiency. The proposed topology is explained in detail and analyzed with the quantitative approach to verify the improvement of system efficiency and power density in the DC-DC power conversion unit: 99.5% efficiency and 3.3kW rated power for 7.5kW PV and 2.5kW battery system. Also, the steady-state operation of the proposed universal optimizer is verified through the controller hardware-in-the-loop test.**

Keywords—battery-ready, dual active bridge dc-dc converter, energy storage, grid-connected pv inverter, high efficiency, partial power processing, seamless pv-battery integration, universal optimizer.

I. INTRODUCTION

Due to the intermittent nature of solar photovoltaic (PV) energy sources and concerns regarding electricity demand and energy saving, integration of energy storage system with the PV generation system has received significant encouragement in residential and commercial grid-tied applications [1]-[4]. In most of the conventional grid-tied PV generation system, legacy PV power electronics topologies [5] are used for the integration of energy storage as shown in Fig. 1: a) AC parallel integration [6], [7], b) DC parallel integration [8], [9], c) in-line integration [10], [11], and d) AC series integration [12]. For the integration of energy storage system, voltage-amplification power electronics stages, high-voltage energy storage sources, or reconfiguration of system architecture are required to cope with different system parameters including limited roof area, weather condition changes, different PV string voltage and power.

This paper proposes a novel battery-ready PV power electronics topology with a partially-rated universal optimizer. In this topology, a seamless integration of a battery into the grid-connected rooftop PV system is available. By applying DC series-connection between the PV string and the battery, the battery helps the PV system to have more flexibility in maintaining its grid-connection with different system characteristics reducing PV system's output voltages; for example, a small number of PV panels, solar irradiance drop, ambient temperature rise, and low voltage and low power system design. These benefits are enabled by adopting partial power processing technique which also improves system efficiency and power density [13]-[17]. In the proposed topology, a dual active bridge (DAB) DC-DC converter is applied to configure partially-rated power electronics system for both PV and battery output power with bi-directional power flow, galvanic isolation, a high voltage boosting gain, and high conversion efficiency [18], [19]. The proposed topology is explained in details with the system characteristics and is analyzed with the quantitative approach regarding the system efficiency and power density improvements under different operational modes: PV-only mode and PV-battery mode. Also, feasibility and performance of the proposed universal optimizer in the steady-state operation is analyzed and verified through the controller hardware-in-the-loop (CHIL) test.

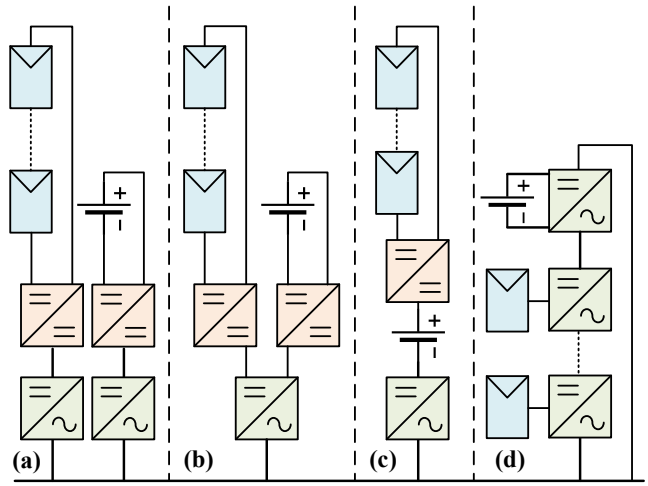

Fig. 1. State-of-the-art of battery integration methods for grid-connected PV inverters in residential and commercial applications (a) AC parallel integration, (b) DC parallel integration, (c) in-line integration, (d) AC series integration.

The paper is organized as follows: In Section II, the proposed PV-battery integration strategy and system architecture are presented. In Section III, the proposed topology for the battery-ready universal optimizer is discussed with a quantitative approach in different operation modes. Section IV provides the CHIL experiment results and discussions followed by Section V as a conclusion.

II. Proposed PV-Battery Integration Strategy and System Architecture

This paper investigates a novel PV string inverter system allowing a seamless integration of a battery for residential and commercial grid-connected rooftop applications. The proposed approach is to connect a battery to the PV string in series, the DC series integration, as shown in Fig. 2. In this method, the battery supports the PV string in maintaining the grid-connection by adding its output voltage to the PV string output voltage. Therefore, a voltage amplification power electronics stage, an essential device for the legacy PV inverter systems, is not required to cope with different system characteristics including roof area, cabling limitations, weather conditions, and PV string voltage and power. However, since the PV output current and the battery output current are the same in the series-connection, the battery unit discharges its power continuously as long as the PV string generates the output power. Therefore, compensating current needs to be injected into the PV-battery coupling point to guarantee the robust controls of the battery output power: battery charging and discharging control. Adopting partial power processing technique [13]-[17], the authors propose a partially-rated power electronics module (and its control) functioning as the compensator of battery discharging power and the universal optimizer for the PV-battery integration. The proposed universal optimizer has two operation modes: A) PV-only and B) PV-battery.

A. PV-only mode

In the commercially-available PV inverter architecture, a DC-DC converter, the legacy PV optimizer, is used for PV output voltage amplification and processes 100% of the PV output power as shown in Fig. 3(a). Instead of having the fully-rated legacy PV optimizer, a partially-rated PV optimizer can be replaced to compensate for the PV output voltage deficit by adding a series voltage, V_{SE}, to the PV string voltage as depicted in Fig. 3(b). By adding a direct power path between the PV string and the DC-AC inverter, the partially-rated DC-DC optimizer processes only the portion of the PV power, but still can deliver 100% of the PV power to the DC-AC inverter. The partially processed power rate (PPPR) for the PV power is proportional to the ratio between the series voltage and the PV output voltage as

$$PPPR_{PV} = \frac{V_{SE}}{V_{PV}} \cdot \tag{1}$$

The optimizer can perform PV maximum power point tracking (MPPT) control by regulating the series voltage when the DC bus voltage, V_{bus}, is constantly maintained by the grid-tied inverter. Besides, further circuit optimization is proposed in this paper to maximize the system efficiency, to reduce the voltage stress, and to achieve partial power processing operation for both PV and battery system as presented in Fig. 3(c): the universal optimizer. A partial amount of the compensating power is processed through the universal

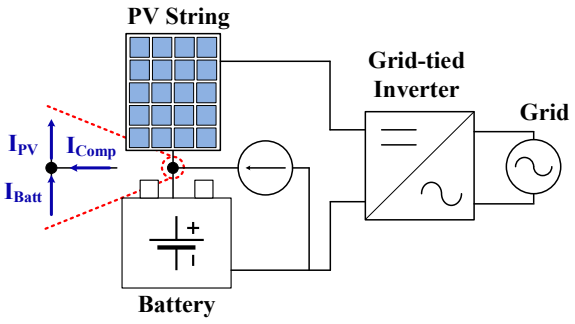

Fig. 2. The proposed approach: DC Series integration.

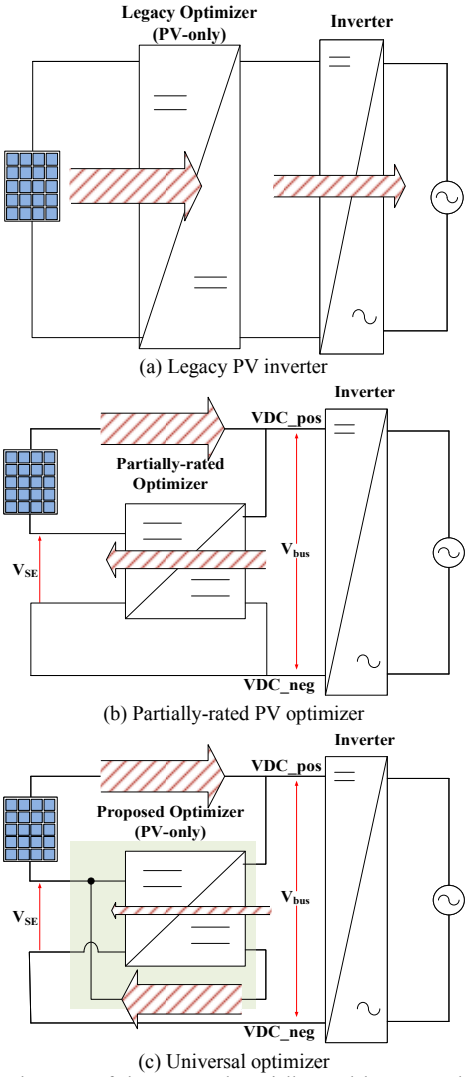

Fig. 3. Development of the proposed partially-rated battery-ready universal optimizer in PV-only mode.

optimizer by having the series-connection on the DC-bus side with the optimizer input voltage and the series voltage. The PPPR for the battery power is proportional to the ratio between the PV voltage and the DC bus voltage as

$$PPPR_{Batt} = \frac{V_{bus} - V_{SE}}{V_{bus}} = \frac{V_{PV}}{V_{bus}}. \quad (2)$$

Consequently, the optimization of the minimum rated power of the proposed DC-DC converter is achieved with the total PPPR, as follows:

$$PPPR_{Total} = PPPR_{PV} \times PPPR_{Batt} = \frac{V_{SE}}{V_{PV}} \times \frac{V_{PV}}{V_{bus}} = \frac{V_{SE}}{V_{bus}} \quad (3)$$

$$P_{optimizer} = \frac{P_{PV} \times PPPR_{Total}}{\eta_{optimizer}} \quad (4)$$

where $\eta_{optimizer}$ is the power conversion efficiency of the DC-DC converter used for the universal optimizer.

In other words, the PV system can use a DC-DC converter with a low-rated power, which represents the reduced size and cost, and the improved power density. Furthermore, due to the low amount of system power loss caused by the reduced rated power of the DC-DC converter, the partially-rated PV optimizer provides higher system efficiency as

$$P_{loss} = P_{optimizer}\left(1 - \eta_{optimizer}\right) \quad (5)$$

$$\eta_{PV} = \frac{P_{PV} - P_{loss}}{P_{PV}} = 1 - \frac{PPPR_{Total}}{\eta_{optimizer}}(1 - \eta_{optimizer}). \quad (6)$$

B. PV-battery mode

In the proposed universal optimizer, the battery integration can be easily achievable by connecting the battery to the open terminals between the PV string and the ground directly as shown in Fig. 4, without additional power electronics stage. In this architecture, the battery can be used as a power source and a PV voltage compensator, simultaneously. Unlike the PV-only mode, the series voltage, which is compensating the PV output voltage deficit, is enforced to be almost constant of the battery voltage as

$$V_{SE} = V_{Batt}. \quad (7)$$

Therefore, the DC bus voltage is regulated to perform PV MPPT control in this mode. Also, the optimizer controls its output current at the T-node in Fig. 4 to perform battery charging and discharging control. For example, if the battery is not engaging in the charging or discharging control and only supporting the PV output voltage, the optimizer output current

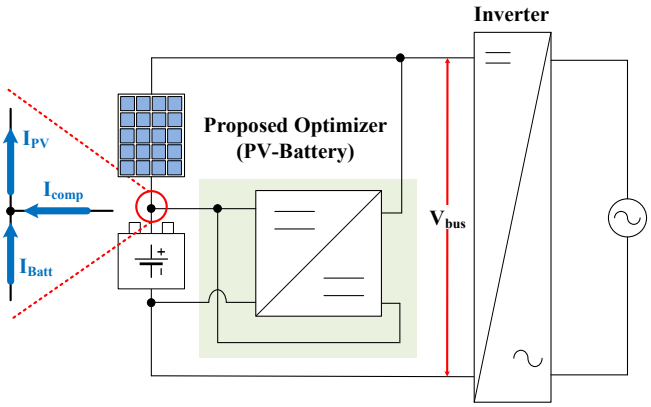

Fig. 4. The proposed battery-ready universal optimizer in PV-battery mode.

will be controlled as $I_{cont}=I_{PV}$ and $I_{Batt}=0$. In the battery charging mode, the optimizer output current will be increased to inject more current into the T-node. Also, in the battery discharging mode, the optimizer output current will be decreased. Since the PPPR of the proposed optimizer is proportional to the battery voltage as

$$PPPR_{Total} = PPPR_{PV} \times PPPR_{Batt} = \frac{V_{Batt}}{V_{PV}} \times \frac{V_{PV}}{V_{bus}} = \frac{V_{Batt}}{V_{bus}}, \quad (8)$$

the battery voltage/power affects the system efficiency and needs to be sized to optimize the impact on the entire system.

III. Proposed Power Electronics Topology and a Cast Study

Fig. 5 shows the proposed power electronics topology for the universal optimizer. A DAB DC-DC converter using wide bandgap semiconductor devices is designed for the proposed optimizer. The DAB converter provides bi-directional power flow, galvanic isolation, a high voltage boosting gain between its input and output, and easiness of realizing soft-switching which is related to low switching loss [18], [19]. Therefore, high conversion efficiency, small volume, and high power density can be achieved in the DAB with high switching frequency. For the DC-AC inverter stage, a state-of-the-art DC-AC inverter is considered in this architecture. Table I presents a case study of the total system properties with and without a battery. A 7.5kW PV string and a 2.5kW battery are

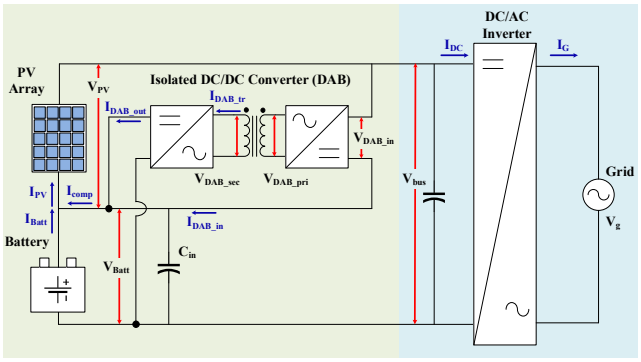

Fig. 5. Proposed topology for the universal optimizer.

TABLE I. SYSTEM PROPERTIES – A CASE STUDY.

System Parameters			
PV	MPP PWR	2x 7.5kW	
	Panels	10x3 PV Panels Each	
	MPP Volt.	318.4V	
Battery	Power	2x 2.5kW	
	Energy	2x 13.2kWh	
	Voltage	50V	
Grid	Voltage	3-φ UG/208V_{RMS}	
A PV/Battery Universal Optimizer			
Operation Mode		PV Only	PV+Battery
PV Output Voltage		318.4V	318.4V
Series Voltage		81.6V	50V
Nominal Rated Power		1.5kW (21%)	3.3kW (43%)
Absolute η_{DAB}		97.5%	97.5%
$\eta_{optimizer}$	PV Only	99.5%	99.7%
	Discharging	-	99.5%
	Charging	-	99.2%
A DC-AC Inverter			
Rated Power		15kW	15kW
DC-Link Voltage		400V	368.4V
$\eta_{Inverter}$		98.5%	98.5%
Total			
η_{Total}	PV Only	98.0%	98.2%
	Discharging	-	98.0%
	Charging	-	97.9%

considered for the single optimizer unit. A 15kW DC-AC inverter and two optimizers are considered as the commercial rooftop PV-battery inverter application. In this case study, the inverter is connected to the three-phase 208V_{RMS} grid, and PV strings are operating under nominal weather conditions. The 318.4V PV string's maximum power point (MPP) output voltage and 50V battery output voltage are considered as system operating parameters. As a result, the max. 3.3kW optimizer (PPPR: 43%) is required to transfer 5.0kW PV output power to the grid, and 2.5kW PV output power to the battery (charging) for single unit. The battery charging mode is the worst case, which requires maximum power rating, because the optimizer needs to transfer the portion of both the compensating power and the battery charging power. Also, 98.0% of total system efficiency is achieved with 99.5% from the optimizer (when the efficiency of the DAB is assumed as 97.5%) and 98.5% from the DC-AC inverter (State-of-the-art).

IV. RESULTS AND DISCUSSIONS

The proposed power electronics topology for the universal optimizer shown in Fig. 5 is built and run in the Typhoon HIL [20] CHIL test-bed to verify its feasibility with different operation modes. The set-up is composed of a real-time power electronics simulator with 500ns solution time steps and a

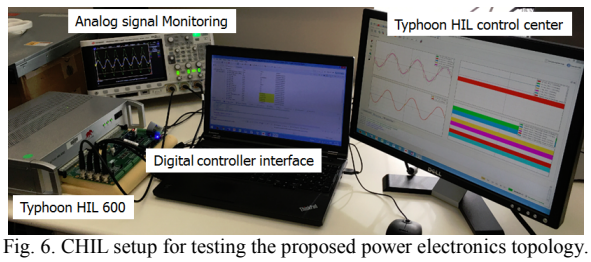

Fig. 6. CHIL setup for testing the proposed power electronics topology.

TABLE II. SYSTME PARAMETERS OF THE DAB DC-DC CONVERTER.

Item	Parameter	Value	Symbol
1	Output Filter capacitor	500uF	C_{out}
2	Transformer primary winding leakage inductance	5uH	L_1
3	Transformer secondary winding leakage inductance	5uH	L_2
4	Transformer primary winding resistance	0.02Ω	R_1
5	Transformer secondary winding resistance	0.02Ω	R_2
6	Transformer turns ratio	318.48:50	n_1:n_2
7	Switching frequency	20kHz	f_{sw}

150MHz microcontroller as shown in Fig. 6. In this work, only the universal DC-DC optimizer is constructed in the real-time power electronics simulator. Instead of having the DC-AC inverter, a constant DC voltage source is considered. Phase-shifted PWM signals are applied to operate the DAB DC-DC converter. The system parameters are presented in Table II.

A. PV-only mode

The CHIL experiment results of the PV-only mode operation of the proposed universal optimizer under nominal PV operating condition are presented in Fig. 7. To deliver 7.3kW PV output power to the 400V DC source which is corresponding to the DC bus of the DC-AC inverter, 1.8kW electric power is processed through the DAB (PPPR=25%) by regulating the DAB's output voltage (the series voltage) as

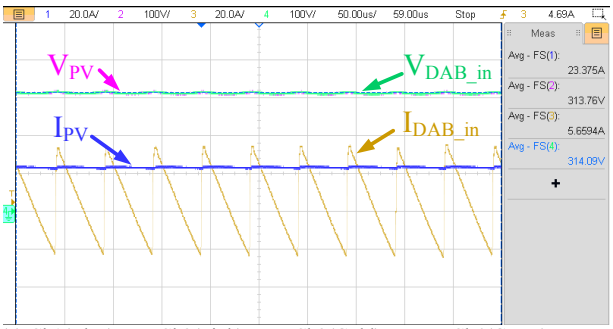

(a) Ch1(Blue): I_{PV}, Ch2(Pink): V_{PV}, Ch3(Gold): I_{DAB_in}, Ch4(Green): V_{DAB_in}

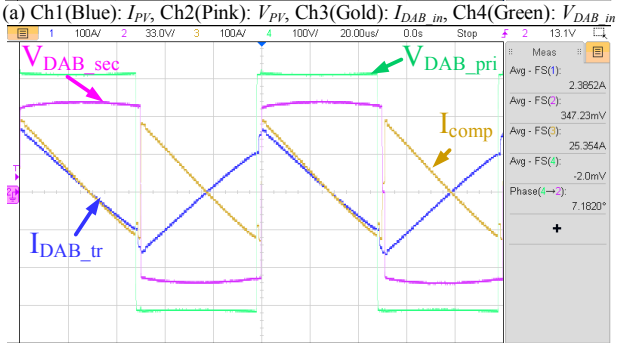

(b) Ch1(Blue): I_{DAB_tr}, Ch2(Pink): V_{DAB_sec}, Ch3(Gold): I_{comp}, Ch4(Green): V_{DAB_pri}

Fig. 7. CHIL Experiment results: PV-only mode at the MPP of the PV string; 7.3kW PV output power and 1.8kW power rating of the DAB.

86.24V with 7.2° degrees phase-shift between the primary and the secondary voltages of the high-frequency transformer in the DAB. In these CHIL results, it is seen that the DAB's input and output current ripples are significant, especially the output current ripple (around 300A) due to the small output voltage. This current ripple can be reduced by adopting higher switching frequency (>200kHz) in a real-hardware system, advanced switching control strategies, and active clamping approach. This can be our future challenges to develop the proposed optimizer. In the CHIL set-up, the higher switching frequency, the lower resolution output waveform due to the limitation of the digital-to-analog conversion circuit in the real-time simulator.

B. PV-battery mode

Once the battery is integrated to the proposed universal optimizer, there are three sub-operating modes. Fig. 8 presents the zero battery current mode. The zero battery current mode is the same as the PV-only mode introduced in the previous section. The only difference is the magnitude of the series voltage. In this case, the series voltage is equal to the battery voltage. Therefore, system efficiency and size are dependent on the battery selection. To deliver 7.5kW PV output power to the 368.5V DC source which is corresponding to the DC bus of the DC-AC inverter, 1.0kW electric power is processed through the DAB (PPPR=13.3%) with 7.3° degrees phase-shift between the primary and the secondary voltages of the high-frequency transformer in the DAB. Having smaller series voltage reduces the PPPR of the system.

Fig. 9 shows the results of the battery charging mode. By shifting 21.8° degrees more than the previous case, the magnitude of the compensating current is increased. Therefore, the excess current, 50A, will be charged into the battery. Therefore, 3.2kW (PPPR=43%) power is processed through the proposed power electronics converter. This is the most severe case regarding the PPPR.

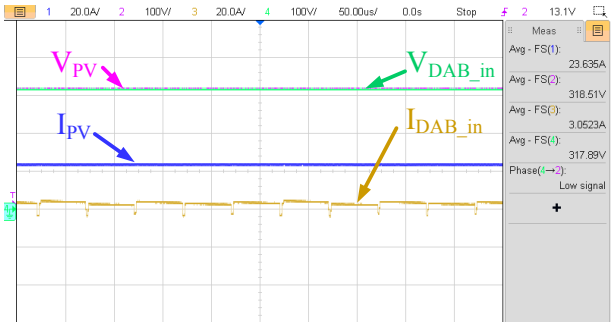

(a) Ch1(Blue): I_{PV}, Ch2(Pink): V_{PV}, Ch3(Gold): I_{DAB_in}, Ch4(Green): V_{DAB_in}

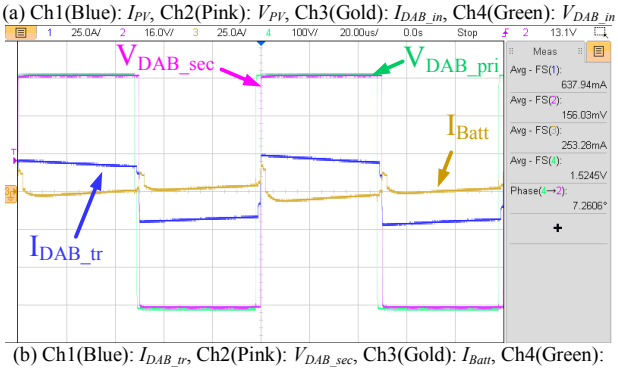

(b) Ch1(Blue): I_{DAB_tr}, Ch2(Pink): V_{DAB_sec}, Ch3(Gold): I_{Batt}, Ch4(Green): V_{DAB_pri}

Fig. 8. CHIL Experiment results: PV-battery mode with the battery current 0A; 7.5kW PV output power and 1.0kW power rating of the DAB.

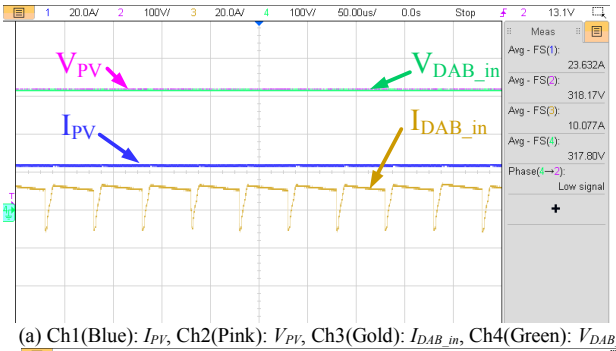

(a) Ch1(Blue): I_{PV}, Ch2(Pink): V_{PV}, Ch3(Gold): I_{DAB_in}, Ch4(Green): V_{DAB_in}

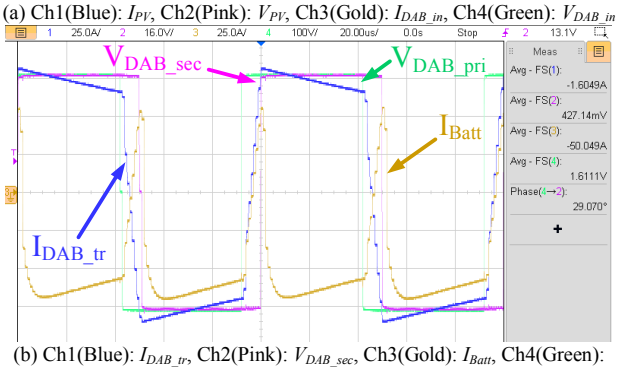

(b) Ch1(Blue): I_{DAB_tr}, Ch2(Pink): V_{DAB_sec}, Ch3(Gold): I_{Batt}, Ch4(Green): V_{DAB_pri}

Fig. 9. CHIL Experiment results: PV-battery mode with the battery charging 50A; 7.5kW PV output power and 3.2kW power rating of the DAB.

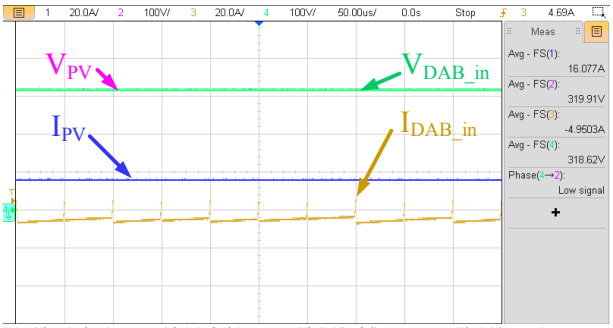

(a) Ch1(Blue): I_{PV}, Ch2(Pink): V_{PV}, Ch3(Gold): I_{DAB_in}, Ch4(Green): V_{DAB_in}

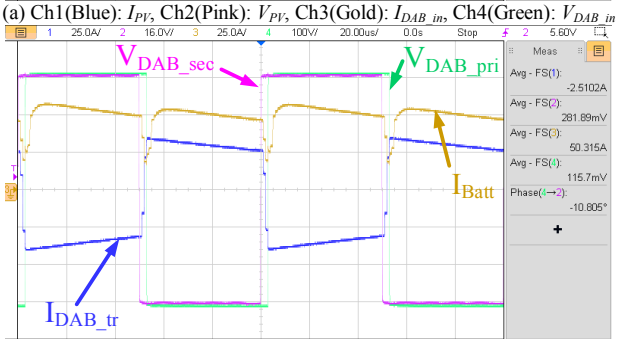

(b) Ch1(Blue): I_{DAB_tr}, Ch2(Pink): V_{DAB_sec}, Ch3(Gold): I_{Batt}, Ch4(Green): V_{DAB_pri}

Fig. 10. CHIL Experiment results: PV-battery mode with the battery discharging 50A; 5.1kW PV output power and 1.6kW power rating of the DAB.

Fig. 10 shows the battery discharging mode. In this case, the phase-shift operation is reversed. With the amount of the PV output current, the battery output current is discharged through the PV power loop until the compensating current becomes zero. If the compensating current is less than zero, the battery discharging current is conducting through the DAB and the battery partial power processing line. This battery partial power processing architecture provides higher efficiency, higher power density, and smaller power rating for the battery output power. Due to the power limit of the DC-AC inverter system (7.5kW per each unit), 5kW PV output power and 2.5kW battery discharging power are considered. By shifting -10.8° degrees between the primary and the secondary voltages of the high-frequency transformer in the DAB, 50A battery current is discharged, and 1.6kW (PPPR=21%) power is processed.

V. CONCLUSIONS

In this paper, a new grid-tied battery-ready PV inverter architecture for residential and commercial applications was proposed. With the proposed PV-battery inverter topology, a seamless integration of battery is available with the universal optimizer. The universal optimizer uses the partial power processing strategy which enables wide PV input voltage range of the PV-battery inverter system, and improving its efficiency and power density. Based on the numerical analysis and the CHIL experiment results, 2% of efficiency improvement and 67% of rated power reduction in the DC-DC converter were achieved. Comparative analysis and optimization on the efficiency and size of the proposed battery-ready PV inverter architecture will be provided in future work.

ACKNOWLEDGMENT

This work is supported by Energy Production and Infrastructure Center (EPIC), Electrical and Computer Engineering Department at the University of North Carolina at Charlotte.

REFERENCES

[1] C. A. Hill, M. C. Such, C. Dongmei, J. Gonzalez, and W. M. Grady, “Battery energy storage for enabling integration of distributed solar power generation,” *IEEE Trans. Smart Grid*, vol. 3, no. 2, pp. 850–857, Jun. 2012.

[2] T. D. Hund, S. Gonzalez, and K. Barrett, “Grid-tied PV system energy smoothing,” *in Proc. 35th IEEE Photovoltaic Specialists Conf. (PVSC)*, Honolulu, HI, USA, Jun. 20–25, 2010, pp. 2762–2766.

[3] M. J. E. Alam, K. M. Muttaqi, and D. Sutanto, "A Novel Approach for Ramp-Rate Control of Solar PV Using Energy Storage to Mitigate Output Fluctuations Caused by Cloud Passing,” *IEEE Transactions on Energy Conversion*, vol. 29, no. 2, pp. 507-518, Mar. 2014.

[4] J. Traube, F. Lu, and D. Maksimovic, “Mitigation of solar irradiance intermittency in photovoltaic power systems with integrated electric—Vehicle charging functionality,” *IEEE Trans. Power Electron.*, vol. 28, no. 6, pp. 3058–3067, Jun. 2013.

[5] S. B. Kjaer, J. K. Pedersen, and F. Blaabjerg, "A review of single-phase grid-connected inverters for photovoltaic modules," *IEEE transactions on industry applications*, vol. 41, no. 5, pp. 1292-1306, Sep. 2005

[6] V. Vega-Garita, L. Ramirez-Elizondo, G. R. C. Mouli, and P. Bauer, "Review of residential PV-storage architectures," *in Proc. Energy Conference (ENERGYCON), 2016 IEEE International*, Leuven, Belgium, Apr. 2016, pp. 1-6.

[7] S. Kouro, J. I. Leon, D. Vinnikov, and L. G. Franquelo, "Grid-connected photovoltaic systems: An overview of recent research and emerging PV converter technology," *IEEE Industrial Electronics Magazine*, vol. 9, no. 1, pp. 47-61, Mar. 2015.

[8] S. Mishra, D. Pullaguram, S. A. Buragappu, and D. Ramasubramanian, "Single-phase synchronverter for a grid-connected roof top photovoltaic system," *IET Renewable Power Generation*, vol. 10, no. 8, pp. 1187-1194, May 2016.

[9] B. I. Rani, G. S. Ilango, and C. Nagamani, "Control strategy for power flow management in a PV system supplying DC loads," *IEEE Transactions on industrial electronics*, vol. 60, no. 8, pp. 3185-3194, Aug. 2013.

[10] Y. Lo, T. Lee, and K. Wu, "Grid-connected photovoltaic system with power factor correction," *IEEE Transactions on Industrial Electronics*, vol. 55, no. 5, pp. 2224-2227, May 2008.

[11] S. J. Chiang, K. T. Chang, and C. Y. Yen, "Residential photovoltaic energy storage system," *IEEE Transactions on industrial electronics*, vol. 45, no. 3, pp. 385-394, Jun. 1998.

[12] N. Kim and B. Parkhideh, "Ramp-rate control strategy for distributed PV-ESS AC-stacked inverter architecture," *in Proc. Power Electronics for Distributed Generation Systems (PEDG), 2017 IEEE 8th International Symposium on*, Florianópolis, Brazil, Apr. 2017, pp. 1-6.

[13] J. P. Lee, B.D. Min, T.J. Kim, D.W. Yoo, and J.Y. Yoo, "A novel topology for photovoltaic DC/DC full-bridge converter with flat efficiency under wide PV module voltage and load range," *IEEE Transactions on Industrial Electronics*, vol. 55, no. 7, pp. 2655-2663, Jul 2008.

[14] B.D. Min, J.P. Lee, J.H. Kim, T.J. Kim, D.W. Yoo, and E.H. Song, "A new topology with high efficiency throughout all load range for photovoltaic PCS," *IEEE Transactions on Industrial electronics*, vol. 56, no. 11 pp. 4427-4435, Nov. 2009.

[15] J.P. Lee, B.D. Min, T.J. Kim, D.W. Yoo, and J.Y. Yoo, "Input-series-output-parallel connected DC/DC converter for a photovoltaic PCS with high efficiency under a wide load range," *Journal of Power Electronics*, vol. 10, no. 1, pp. 9-13, 2010.

[16] M. O. Badawy, A. S. Yilmaz, Y. Sozer, and I. Husain, "Parallel power processing topology for solar PV applications," *IEEE Transactions on Industry Applications*, vol. 50, no. 2, pp. 1245-1255, Mar. 2014.

[17] H. Dehbonei, S. R. Lee, and S. H. Ko, "Direct energy transfer for high efficiency photovoltaic energy systems part II: experimental evaluations," *IEEE Transactions on Aerospace and Electronic Systems*, vol. 45, no. 1, Jan. 2009.

[18] B. Zhao, Q. Song, W. Liu, and Y. Sun, "Overview of dual-active-bridge isolated bidirectional DC–DC converter for high-frequency-link power-conversion system," *IEEE Transactions on Power Electronics*, vol. 29, no. 8, pp. 4091-4106, Aug. 2014.

[19] F. Krismer and J. W. Kolar, "Efficiency-optimized high-current dual active bridge converter for automotive applications," *IEEE Transactions on Industrial Electronics*, vol. 59, no. 7, pp. 2745-2760, Jul. 2012.

[20] Typhoon HIL, Inc., MA, USA. *Typhoon HIL Real-time Hardware-in-the-Loop (HIL) simulation platform, Typhoon HIL Control Center Release 2017.3.* (2017) [Online]. Available: https://www.typhoon-hil.com/doc/brochures/Typhoon_HIL600_Brochure_downloadable.pdf, Accessed on: Nov. 14, 2017.